

Investigating ultra-thin 4H-SiC AC-LGADs for superior radiation-hard timing applications

Jaideep Kalani^a, Saptarshi Datta^{b,c}, Ganesh J Tambve^{c,d}, Prabhakar Palni^a

^a*School of Physical Sciences, Indian Institute of Technology, Mandi, 175005, Himachal Pradesh, India*

^b*School of Physical Sciences, National Institute of Science Education and Research, Bhubaneswar, 752050, Odisha, India*

^c*Homi Bhabha National Institute, Mumbai, 400094, Maharashtra, India*

^d*Centre for Medical and Radiation Physics, National Institute of Science Education and Research, Bhubaneswar, 752050, Odisha, India*

Abstract

The Low Gain Avalanche Diodes (LGADs) are promising particle detectors for timing resolution better than 50 ps under a high radiation environment. This study investigates n-in-p LGAD architecture, focusing on ultra-thin sensors of thickness less than 50 μm using the WeightField2 program. The capabilities of WeightField2 are demonstrated by comparing its results with irradiation measurements from an FBK LGAD wafer, showing good agreement across unirradiated and neutron-irradiated conditions. This paper presents device simulations in High Luminosity LHC conditions (lifetime integrated fluence $O(10^{14})$ $\text{n}_{\text{eq}} \text{cm}^{-2}$, temperature ≈ 243 K), and taking into account radiation damage, gain reduction due to fluence, and lattice defects. It is shown that a 20 μm thick sensor achieves the best timing performance. Among Silicon (Si), Diamond (C), and 4H-Silicon Carbide (4H-SiC), we found 4H-SiC to be the most promising: it provides the highest gain value for a fixed thickness and gain implant layer configuration, and best retains high charge collection value and timing capability under increasing fluence up to 50×10^{14} $\text{n}_{\text{eq}} \text{cm}^{-2}$. A time resolution less than 25 ps is reported with different gain implant concentrations for a 20 μm 4H-SiC sensor. This work presents the potential of SiC-based LGADs in high-radiation collider environments.

Keywords:

AC-LGAD, UFSD, Radiation Hardness, Silicon Carbide, Time Resolution

1. Introduction

The High-Luminosity Large Hadron Collider (HL-LHC) project aims to increase the instantaneous luminosity to $\approx 7.5 \times 10^{34} \text{ cm}^{-2}\text{s}^{-1}$ [1]. These upgrades, including other future high-energy physics experiments ([2], [3], [4]) seeking larger event statistics, will lead to severe pile-up conditions. The Low Gain Avalanche Diodes (LGADs) offer a timing resolution of approximately 50 ps or lower ([5], [6]), along with spatial resolution below 100 μm (depending on pixel dimensions [7]). The LGADs provide an effective solution to mitigate high pile-up scenarios. Therefore, this technology has been qualified for use in the MIP Timing Detector (MTD) detector ([8],[9]) of CMS and the High Granularity Timing Detector (HGTD) [10] of ATLAS for HL-LHC operations.

The LGADs outperform standard PIN diodes by introducing an extra gain layer for controlled avalanche multiplication of charge carriers in addition to the drift and diffusion mechanisms. The gain layer is usually a

thin, highly doped region with a moderate gain factor (gain $\sim 10 - 30$). This increases the signal amplitude while preserving a high signal-to-noise ratio without the dangers of noise-induced breakdown. A key advancement is the AC-LGAD (AC-coupled) design (Figure 1), which mitigates DC-LGAD [11] (DC-coupled) limitations such as charge-sharing inefficiencies and pixelation constraints due to direct coupling of the readout to the gain layer. In AC-LGADs, the readout is capacitively coupled to the gain layer through an insulating layer; this enables continuous gain layer (increasing fill factor), and improved spatial resolution (much lower than pixel size). These, along with compatibility with modern semiconductor processing techniques, make AC-LGADs suitable for high-granularity, high-resolution timing and tracking (4D) detectors. [12]

This study examines the time resolution (σ_t) of an LGAD as a function of operational conditions like bias voltage and radiation damage, including device characteristics like gain implant (G.I.) layer concentration,

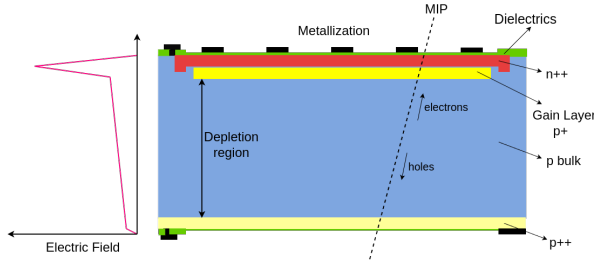


Figure 1: A typical AC-LGAD architecture

thickness, and bulk material. This work evaluates three different bulk materials, including 4H Silicon Carbide (4H-SiC), where H denotes hexagonal symmetry and a 4-layer per unit cell poly-type of SiC ([13] [14]). It is well-suited for detector applications due to high saturation drift velocity of carriers, high bandgap (so low intrinsic charge concentration), high breakdown field, and good thermal conductivity. The operational qualities for a 4H-SiC-based LGAD are presented and compared to a Si-based LGAD with similar configurations to demonstrate the former's superiority as a radiation-hard 4D detector. Throughout this study, SiC is used as an alias for the 4H-SiC polytype for brevity.

1.1. Theoretical framework of the LGAD mechanism

The impinging minimum ionising particle (MIP) produces primary e^-h^+ pairs while passing through the sensor bulk; these primary carriers further produces cascade of secondary carriers while passing through the gain layer. A calculation using the Shockley-Ramo theorem ([15],[16],[17]) gives the net current (in full signal time) as: $I \propto N_{gen} q_0 v_{sat} (G/d)$ [18]. Here N_{gen} is the number of primary charge carriers generated by the MIP, q is the carrier's charge, v_{sat} is the saturation velocity of the charge carrier in the sensor bulk, G is the gain value of the sensor, and d is the thickness of the sensor. This is the key advantage of the LGAD design over a typical semiconductor sensor with a diode-like design. Clearly the signal is amplified from $N_{gen} q_0$ for a typical diode to a larger factor for LGADs.

In LGADs, impact ionisation is the crucial mechanism providing the gain factor. The Massey model [19] is an empirical framework used to simulate such a mechanism. The ionisation rate, characterised by the ionisation coefficients α_n and α_p for electrons and holes, respectively, follows an empirical relationship:

$$\alpha_{n,p}(T) = A_{n,p}(T) \exp\left(-\frac{B_{n,p}(T)}{E}\right),$$

where $A_{n,p}(T)$ and $B_{n,p}(T)$ are material-dependent parameters that account for temperature variations, and

E is the local electric field. Furthermore, material-dependent parameter $B_{n,p}(T)$ is represented as $B_{n,p}(T) = C_{n,p} + D_{n,p} \cdot T$. These $A_{n,p}$, $C_{n,p}$, and $D_{n,p}$ are six model parameters which are fine-tuned by comparing simulations and empirical data. Corrections dependent on temperature and doping concentration are introduced to make the model more accurate. Comparative TCAD studies ([20], [21]) demonstrate that the Massey model of LGAD mechanism agrees with experimental data across multiple regimes, including gain versus bias voltage, gain versus temperature, and breakdown voltage predictions. We used the Massey model in all simulations and the model parameters are fixed within the WF2 simulation framework as per published default values of the Massey model [19].

1.2. Radiation damage in LGAD

The radiation damage in an LGAD is broadly of two categories: surface damage and bulk damage [22]. The former is due to ionisation energy loss; the particle traversing through the sensor ionises the sensor bulk by energy deposition and forms e^-/h^+ pairs. Some of these form at the interface of the sensor bulk and the oxide layer, and cannot recombine properly, leaving trapped charges at the interface.

A fraction of the non-ionising energy loss, causes bulk damage to the lattice. The impinging particle, like hadrons, forms Frankel pairs [23]. Some of these pairs get recombined, while others migrate through the lattice and can interact with the other impurities present in the bulk, producing point defects. Furthermore, these migrating Frankel pairs have enough energy to create further ionisation and atomic displacements. Here the radiation damage is measured in equivalent 1 MeV neutron fluence ($1 \text{ MeV } n_{eq} \text{ cm}^{-2}$) [5].

Due to radiation exposure, the dopant (acceptors in this case) concentration can be affected by acceptor removal. This process is incorporated into radiation damage simulations. Acceptor removal is a bulk phenomenon caused by radiation-induced defects that deactivate acceptor atoms in the gain layer, leading to a reduction in the effective doping concentration. This effect becomes more pronounced with increasing fluence and results in a substantial decrease in gain, which in turn degrades charge collection and time resolution [24]. However, SiC-based LGADs exhibit enhanced radiation tolerance and maintain stable gain performance even at high fluences [25].

This study will show how the effects of radiation damage on a sensor can be mitigated by increasing operational bias voltage and maintaining the detector's performance.

1.3. Time resolution

The time resolution of an LGAD for a uniform MIP can be given as [18] [26]:

$$\sigma_t^2 = \left[\left(\frac{V_{th}}{S/t_r} \right)_{RMS} \right]^2 + \sigma_{jitter}^2 + \sigma_{TDC}^2$$

$$\sigma_{jitter} = \frac{N}{S/t_r} \quad \text{and} \quad \sigma_{TDC} = \frac{TDC_{bin}}{\sqrt{12}}$$

where, V_{th} is the threshold voltage, S is the signal amplitude, and t_r is the signal rise time. These all contribute to the first term in the time resolution formula and are collectively referred to as the time walk term ($\sigma_{time\ walk}$) [27]. The σ_{jitter} is the jitter or noise term arising in the signal mainly due to electronics, where N is the rms voltage noise and S/t_r is equivalent to the slew rate at which the detector is performing. TDC_{bin} is the least count of the Time-to-Digital-Convertor. We are not using non-uniform charge deposition in this study. Non-uniform charge deposition (Landau fluctuations) provide an intrinsic limit on time resolution. While doing the WF2 simulations, we do not take this into account to deliver conformal statistics without the need to run longer bunch simulations.

Moreover, slew rate is given as the maximum rate of change of a signal (dV/dt). Higher slew rates create sharper and more distinct signals. However, there is a trade-off that higher slew rates require a higher amplifier bandwidth, which introduces a higher noise level. The optimal slew rate is finite and electronics dependent [17].

2. Simulation methodology

The simulation program WeightField2 (WF2) [28] build 6.0 is used. It allows us to simulate planar LGADs with possibility of choosing DC or AC functionality. We input the thickness of the device, number of strips, width and pitch of each strip, gain layer doping concentration (in units of 10^{16} cm^{-3}) and doping profile (depth location of the gain layer doping). For our study we simulated all devices with gain implant at $0.5 - 1.0 \mu\text{m}$ from the top. Typically we used 3 or 5 strips with the MIP hitting the middle strip at all cases. The doping concentration of the gain layer is varied from $2.5 \times 10^{16} \text{ cm}^{-3}$ to $5.0 \times 10^{16} \text{ cm}^{-3}$ in some studies, while kept constant in others depending on the study, and is described in the respective sections. The gain mechanism is chosen to be the widely accepted ‘‘Massey LGAD model’’ [19]. Typically, the bias voltage is varied with thickness and kept within acceptable operational conditions.

It should be noted that for $20 \mu\text{m}$ thick silicon devices, the operational bias voltage is limited to 250 V; we have used 300 V (a higher value) in Fig 5 only to qualitatively illustrate the trend [41].

To run a simulation we choose ‘‘MIP uniform’’ impinging (ignoring Landau fluctuations) with 57 / 75 e^-/h^+ pairs created per micron, depending on the bulk material [29]. This assumption is standard for the materials studied and allows us to extract the basic features of the signal (analogous to a laser beam study). We always choose neutron irradiation with ‘‘acceptor creation’’ turned on, charge capture efficiency (CCE) or trapping coefficients set to $4.9 \times 10^{-16} \text{ cm}^2/\text{ns}$ and $6.2 \times 10^{-16} \text{ cm}^2/\text{ns}$ (standard values) for e^- and h^+ respectively. We have also studied changes in device properties for change in operational temperature from 243 K (-30°C) to 293 K ($+20^\circ\text{C}$). We have provided the simulation conditions for each study in tables provided in the Appendix.

Weightfield2 employs a silicon-based gain-layer parametrization, where the gain and bulk regions are treated as parts of the same semiconductor bulk differing only by doping concentration. The same gain-layer parametrization are therefore applied to all bulk materials. Consequently, while the gain layer is modeled identically for silicon, 4H-SiC, and diamond, the 4H-SiC results represent a realistic exploration of bulk transport and signal-shaping characteristics under this imposed gain profile. The diamond results, in contrast, are purely conceptual and serve as a comparison of bulk behavior under an assumed gain mechanism. Similarly, since the charge capture efficiency (CCE) or trapping coefficients values of 4H-SiC are unavailable in literature, we set them same as that of silicon. For comparison between multiple devices we match the gain value of the devices. A plotted line of ‘‘constant gain’’ consists of configurations which yield same net charge; this is because we fix the MIP ionisation rate (per micron) in our material and set the gain to be fixed, thus the current is fixed. The acceptor removal mechanism in the gain layer is modelled through the exponential form:

$$N(\Phi) = N_0 e^{-c\Phi}$$

where $N(\Phi)$ is the remaining acceptor concentration after irradiation at fluence Φ , and N_0 is the initial acceptor concentration [30].

The acceptor removal coefficient c is not a constant in WF2, rather, it is calculated dynamically in the software and is a function of the initial gain-layer doping type and the irradiation particle type. In the FBK comparison case, in section 3, WF2 gives $c = 2.2 \times 10^{-16} \text{ cm}^2$, while

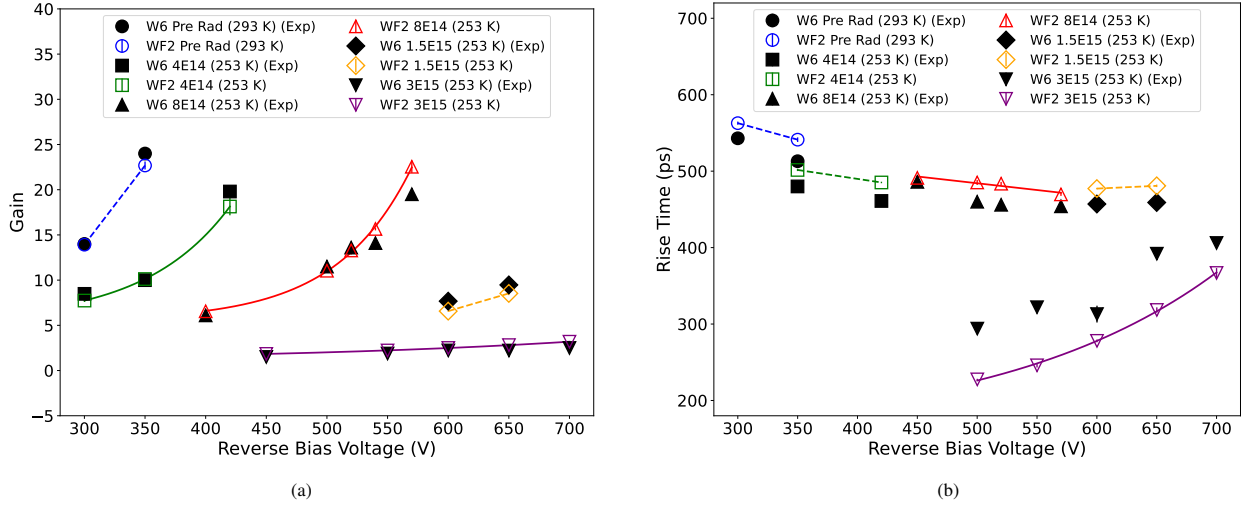


Figure 2: Comparison of WF2 simulated (a) gain and (b) rise time with experimental data from the FBK W6 LGAD sensor [32], for both unirradiated (293 K) and neutron-irradiated (253 K) conditions at various fluence levels. In each plot, the markers labelled as W6 refer to FBK wafer 6 data while markers labelled as WF2 are simulation predictions from WeightField2.

in the study performed with SiC in Section 4.4, WF2 gives $c = 5.57 \times 10^{-16} \text{ cm}^2$. The difference comes from the gain-layer doping type, FBK uses B+C in the gain layer, while in this study B is used as the dopant in the gain layer. More details can be seen in the appendix section for the respective plots.

Moreover, the calculation for time resolution (σ_t) is carried out using a Trans Impedance Amplifier (TI-AMP) for sensor readout at the electronics level, using the standard NA62 model [31]. The time resolution is calculated according to the formula provided in Section 1.3. In our implementation, the quantity V_{th} in the time-walk term is set in the electronics configuration, while the amplitude S and rise time t_r are provided by WF2 after each simulation run. The jitter term is also directly reported by WF2, since it depends on the noise and the effective slew rate of the front-end. The TDC bin is set to 20 ps here, following [27].

WF2 gives gain values with two decimal places, time values with 0.01 ps based on the Q_{tot} calculation, and V_{bias} in steps of 1 V. These should be understood as the granularity of the simulation. The gain implant layer doping concentration is varied up to an order of 10^{13} cm^{-3} , which is negligible (0.1%) compared to the absolute values of the order of 10^{16} cm^{-3} .

3. Validation of WF2 predictions with experimental data

To validate the WF2 simulation framework, a comparative study is carried out using results from the FBK

W6 wafer sensor [32]. This device is a 60 μm thick silicon DC LGAD sensor from FBK, with dimensions of $1 \times 1 \text{ mm}^2$. The whole setup was kept at -27°C . We simulated a device geometry and operational conditions consistent with the W6 FBK UFSD device [32] and compared their reported gain and signal rise time values with the WF2 predictions.

For the FBK W6 device, the exact gain-layer doping concentration is not explicitly reported in the literature. Therefore, it was estimated using the standard $(1/C^2-V)$ method. In that study, the FWHM of the gain-layer profile is provided, and only the central part of the layer is assumed to be fully depleted. Using this information, a range of possible doping concentrations was calculated from

$$N_A = \frac{2 \varepsilon_{Si} V_{GL}}{q t^2}$$

based on the gain layer thickness [30]. Here, t is the effective thickness of gain layer, V_{GL} is the gain-layer depletion voltage, ε_{Si} is the permittivity of silicon, and q is the elementary charge. Considering also that WF2 can simulate gain-layer thicknesses up to 0.5 μm , a peak initial acceptor concentration of $4.71 \times 10^{16} \text{ cm}^{-3}$ was chosen at zero fluence as a representative value for the simulations, as it provides the best agreement with the FBK reported gain and signal rise time values. The active layer thickness was set to 55 μm instead of 60 μm , as several studies on FBK W6 wafers indicate that the effective active thickness is about 55 μm after thermal bonding to the substrate [33].

Other structural and operational parameters (e.g.

number of strips and temperature) were taken from the reference study and kept fixed for consistency. The configuration for this simulation is provided in appendix section table 1.

As shown in Figure 2a, the gain (coloured markers) closely aligns with the reported experimental measurements (black markers), both demonstrating a comparable exponential increase with bias voltage. Furthermore, the expected reduction in gain with increasing fluence, along with gain recovery at higher bias voltages, is well reproduced by the simulation. A similar comparison is carried out for the signal rise time as a function of bias voltage. The rise time is defined as the time between 10% and 90% of the peak signal amplitude (same as CFD technique used in published data). As can be seen in the Figure 2b, trend of decreasing rise time with increasing bias is predicted correctly by WF2.

The WF2 measurements shown in Figure 2a and Figure 2b are fitted, except for the data with only two points, which are connected by a dashed line. The overall agreement of WF2 predictions with published sensor data confirms the capability of WF2 to reliably capture key features of the internal charge multiplication mechanism in LGADs.

4. Results and discussion

We investigated different material choices for the sensor bulk followed by a study on preferred thickness. Further, we present detailed characterisation of the detector's electrical behaviour, signal response, performance metrics under various operating conditions, including high radiation dosage.

4.1. Choice of sensor bulk material

We investigated devices with bulk materials Silicon (Si), 4H-SiC, and Diamond. We noticed a significant performance difference in the ultra-thin range (thickness 20 μm). The bias voltage is kept constant, i.e., 150 V for all three devices while the G.I. concentration is varied to match the gain value of unirradiated devices. Then, for increasing fluence, the variations in both the total charge collection and the time resolution of the devices are studied which is shown in Figure 3.

The choice of material is based on two criteria: maximal total charge collection (Q_{tot}) and retaining good time resolution (σ_t) over an extensive range of fluence, as expected for a tracking detector placed close to the interaction vertex. In Fig 3a, the silicon device and the SiC device have similar Q_{tot} values while the Diamond device performs poorly: at the fluence of $50 \times$

$10^{14} \text{ n}_{eq} \text{ cm}^{-2}$, Si and SiC devices have ~ 2 fC charge collection while Diamond provides less than 1 fC. In Fig 3b, the Diamond device and SiC device have similar σ_t values: they hold a time resolution less than 18 ps, at fluence level of $50 \times 10^{14} \text{ n}_{eq} \text{ cm}^{-2}$, whereas the silicon device's time resolution steeply rises to ~ 23 ps at the same fluence level. Therefore, the results clearly show that only the 4H-SiC material performs well, satisfying both the criteria, making it the best choice for sensor bulk material ([34], [35]).

Diamond generates far fewer electron-hole pairs than silicon, resulting in lower total charge (Q_{tot}), but its exceptional radiation hardness, negligible leakage current, and fast carrier transport yield very short rise times and low noise. Because the jitter term scales as $N/(dV/dt)$, the combination of small N and large dV/dt compensates for the reduced signal amplitude, maintaining timing performance comparable to silicon. The superior timing of 4H-SiC relative to silicon arises from its higher carrier drift velocity at operating fields, larger breakdown field enabling stronger bias.

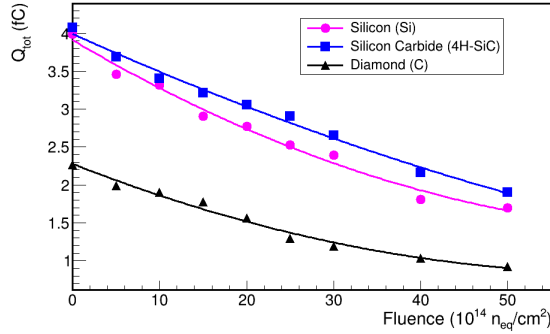
4.2. Thickness dependence of AC-LGAD performance

The simulations are performed for SiC bulk unirradiated AC-LGAD at a constant temperature (243 K) and bias voltage (300 V), and varying thickness. We increased the G.I. doping concentration with increasing thickness to ensure that in unirradiated condition devices of all thickness provide the same gain value. This allowed us to study the dependence of time resolution on sensor thickness as shown in Figure 4.

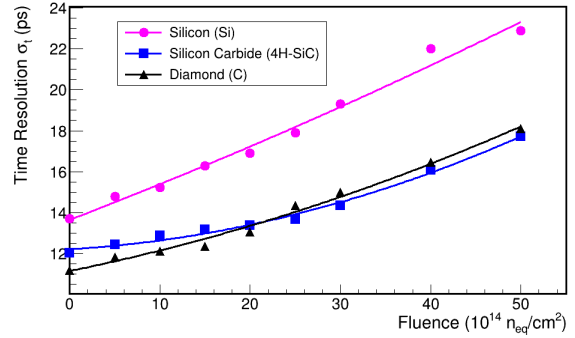
The reduction in the detector thickness from 100 μm to 20 μm results in a relative improvement in time resolution by $\sim 60\%$, for various gain values. This indicates that using thinner sensor, within technological limits, can significantly benefit the timing performance of LGADs.

The timing resolution in LGADs is largely determined by the slew rate, which reflects how fast the signal rises. Even though the charge carriers drift at saturated velocity in all sensor thicknesses, the induced current scales as G/d , as discussed in section 1.1 and section 1.3. Hence, for a fixed gain, higher thicknesses results in a reduced G/d , leading to a lower slew rate and inferior timing resolution.

Figure 5 (top panel) shows the gain as a function of gain layer doping concentration for silicon and silicon carbide bulks, fitted with quadratic curves. The Figure 5 (bottom panel) shows the first derivative of the fits, highlighting the gain sensitivity with respect to doping concentration. Notably, the slope for the SiC bulk is



(a) Charge collected from the LGAD with the TIA decreases with increasing radiation dosage.



(b) The timing capability of detectors worsens with increasing radiation dosage.

Figure 3: Simulation results for detectors of 20 μm thickness and operated at $V_{bias} = 150$ V and temperature of 243 K.

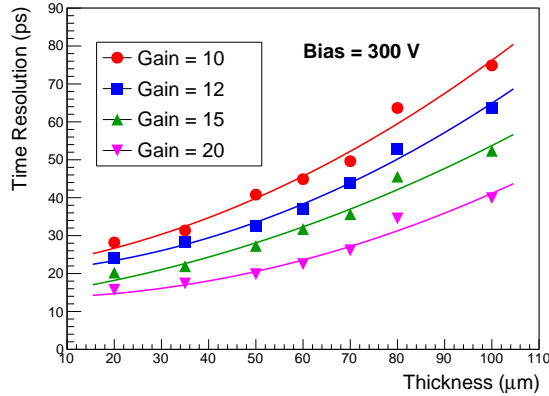


Figure 4: Simulation predictions of time resolution variation as a function of thickness for different fixed-gain SiC bulk AC-LGAD at the constant V_{bias} of 300 V

steeper and increases more rapidly with doping concentration as compared to Si. This indicates a higher gain sensitivity in SiC under fixed thickness and bias conditions. An increase in the gain layer doping concentration enhances the probability of impact ionisation, thereby leading to a higher charge multiplication, i.e. gain. This helps in improving the timing capabilities of the detector. Across all thicknesses, SiC consistently exhibits higher gain than Si, indicating superior charge multiplication efficiency.

In addition, in fig 5, within the considered operating conditions the thickness dependence largely saturates as we go to higher thicknesses, resulting in only minor differences in the G.I. layer doping concentration between the 50 and 70 μm sensors for achieving the same gain, while the 20 μm device shows a lower effective G.I.

doping concentration for achieving the same gain at the same bias.

A comparative study of the performance of the SiC bulk detector relative to the Si bulk is shown in Figure 6, at gain = 10, and under identical physical conditions. The Si bulk AC-LGAD exhibits an improvement of 44% in time resolution, while that of the SiC bulk demonstrates an improvement of 60% while decreasing the thickness from 100 μm to 20 μm .

4.3. Temperature-dependent measurements

The AC-LGADs are highly sensitive to variations in temperature, which can significantly impact their time resolution, charge collection efficiency, and gain characteristics [36]. The readout electronics generates significant heating ([37], [38]) of the sensor. As a result, AC-LGADs experience an increased leakage current due to the localised increase in temperature. The increased leakage current in turn leads to temperature increase. Besides this, there are contributions from shot noise and the Johnson noise; the latter varies as $V_{rms} \propto \sqrt{T}$, where V_{rms} is the r.m.s. voltage due to the noise in the detector [39].

The following measurements present detailed results for the temperature's impact on crucial sensor properties like gain and time resolution. These insights will help to assess the thermal stability of AC-LGADs and thus guide the design of future detectors, optimised for specific operating conditions.

4.3.1. Effect of temperature on gain

Figure 7 illustrates the gain in a SiC bulk (20 μm) as a function of temperature. The gain implant doping concentration is set to $2.301 \times 10^{16} \text{ cm}^{-3}$. The data shows gain profiles at four different bias voltages: 320 V, 340

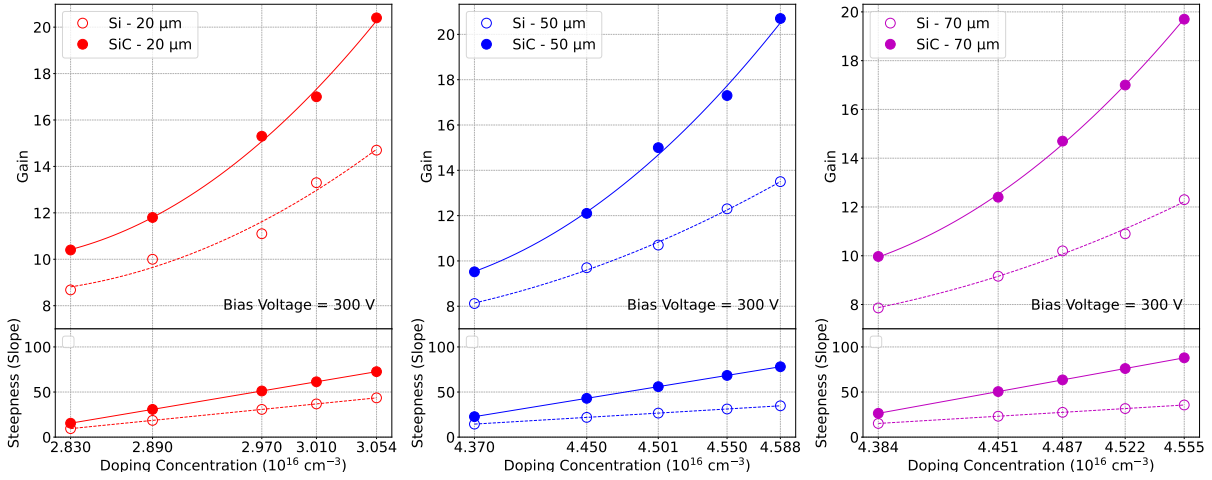


Figure 5: Figures show WF2 predictions of change in gain value of Si and SiC devices with increasing G.I. dopant concentration. *Top*: The variation of gain with increasing doping concentration of the gain layer in 20 μm, 50 μm and 70 μm SiC and Si bulk AC-LGAD with quadratic fits. *Bottom*: First derivative of the quadratic fits of the corresponding curves.

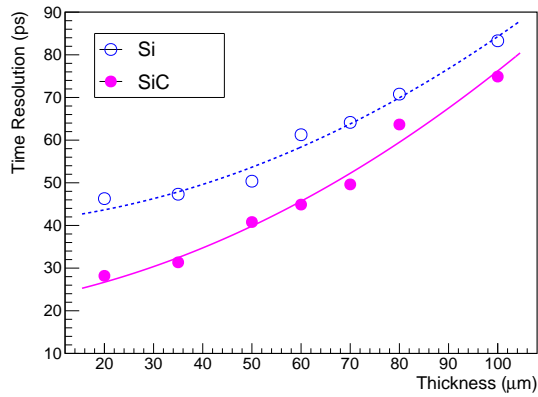


Figure 6: The comparison of simulated time resolution of SiC and Si-bulk AC-LGAD over a thickness range at a fixed gain value of 10. The detectors are operated at fixed bias voltage of 300 V at a temperature of 243 K.

V, 350 V and 360 V. The result indicates a consistent decrease of gain with the increase in temperature, which agrees with the predictions of the Massey model [19]. Therefore, AC-LGADs need to operate at higher V_{bias} with increasing temperature to counteract the decrease in gain value.

4.3.2. Performance of time resolution with temperature

Figure 8 shows the time resolution for a SiC bulk AC-LGAD (G.I. layer doping concentration is 2.301×10^{16} cm⁻³), in solid lines, against the temperature. The data indicates a linearly increasing trend in the time reso-

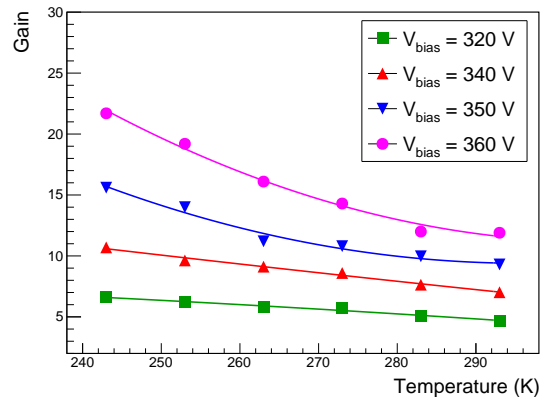


Figure 7: Simulated gain of 20 μm SiC bulk AC-LGAD as a function of temperature for different bias voltages.

lution with temperature, as temperature increased from 243 K to 293 K. For comparison, the study is also conducted for silicon bulk AC-LGAD with the same physical conditions. For every operating bias voltage, the SiC device outperforms the Si device over the entire temperature range. The SiC AC-LGAD shows a decrease in the time resolution by ~ 33% and ~ 48% at bias voltages 320 V and 360 V, respectively, when the temperature is decreased from 293 K to 243 K.

In contrast, the Si bulk AC-LGAD exhibits a decrease in time resolution by ~ 35% and ~ 52% at bias 320 V and 360 V, respectively. A marginal reduction in the percentage drop of time resolution in SiC, directly indicates its stability towards the extreme temperature changes.

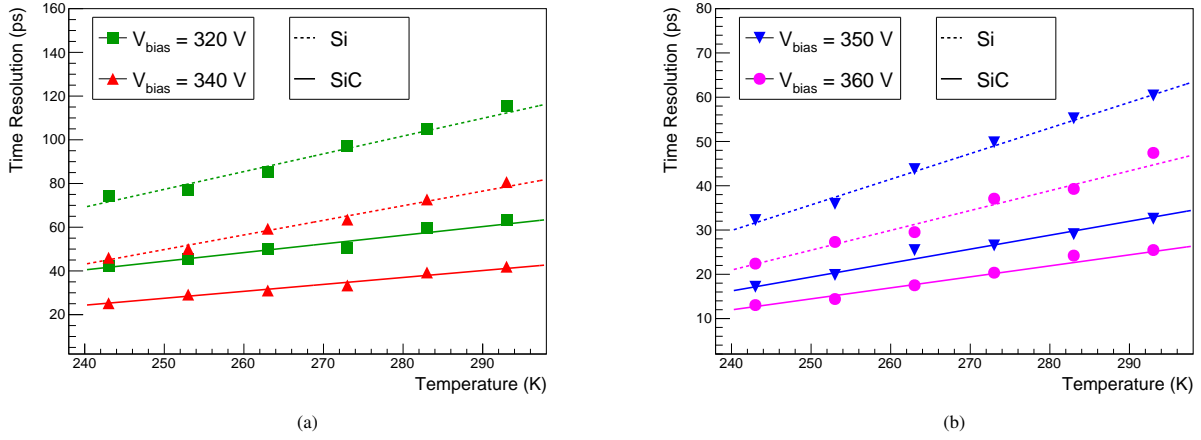


Figure 8: WF2 prediction of timing performance comparison between 20 μm SiC and Si bulk AC-LGAD with increasing temperature at (a) 320 and 340 V and (b) 350 and 360 V.

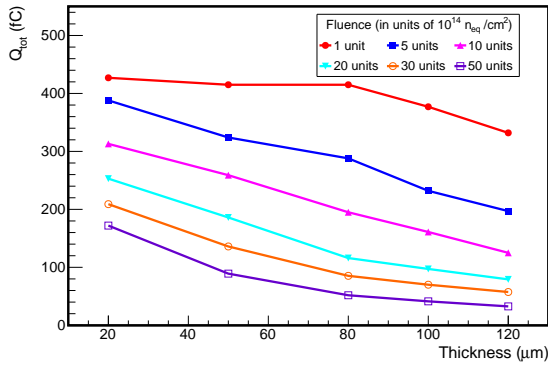


Figure 9: Simulation predictions of variation of Q_{tot} for different sensor thickness with increasing radiation damage. Temperature is set at 253 K and fluence units are in $10^{14} \text{ n}_{\text{eq}} \text{ cm}^{-2}$.

Furthermore, the best time resolution achieved is ~ 13 ps at 243 K for SiC and ~ 22 ps for Si, both at a bias voltage of 360 V. This clearly indicates better temperature stability of SiC, as compared to Si. The higher thermal conductivity of SiC plays a crucial role here; it allows the dissipation of heat evenly, preventing any localised heating, which makes it less sensitive towards temperature changes as shown in figure 8. Moreover, a higher bandgap of SiC also supports in reducing leakage current at elevated temperatures.[35]

4.4. Radiation tolerance of SiC AC-LGADs

Radiation dosage received by the detector is expressed in terms of fluence, in the unit of 1 MeV $\text{n}_{\text{eq}} \text{ cm}^{-2}$. To investigate radiation hardness, SiC AC-LGAD sensor is subjected to various fluence levels,

ranging from unirradiated (zero fluence) to as high as $50 \times 10^{14} \text{ n}_{\text{eq}} \text{ cm}^{-2}$. The study is performed for 20 μm sensor at a constant temperature of 253 K (-20°C) to mimic the beam-pipe temperature [9]. For the thicknesses 20 μm , 50 μm , 80 μm , 100 μm and 120 μm we had the bias voltages as 115 V, 140 V, 142 V, 190 V and 202 V, and the G.I. concentration as (in units of 10^{16} cm^{-3}) as 4.40, 4.82, 4.81, 4.92 and 4.94 respectively. We chose such values to make sure that at Fluence = 0, detectors of all thickness have gain value of 15. Figure 9 shows that the Q_{tot} drops with an increase in fluence levels, for all the sensor thicknesses. This highlights the adverse effects of radiation damage. Radiation damage reduces carrier transport by introducing lattice defects in the bulk, and, reduces gain by neutralising dopants in the G.I. layer [40].

For a particular thickness, with increasing fluence the main reason for reduced charge is the loss of gain due to acceptor removal in the gain layer. Furthermore, the decrease in total collected charge Q_{tot} with increasing thickness (but fixed fluence) is explained by taking into account bulk defects which cause trapping, recombination, finite lifetime, and incomplete depletion. In ideal, defect-free detectors, Q_{tot} always increases with thickness. However with irradiation, bulk defects increase with thickness and thus the Q_{tot} decreases.

4.4.1. Fluence-dependent gain in AC-LGADs

Figure 10 shows that, highly irradiated sensors have much lower gain values for the same bias voltage for a SiC bulk sensor. At a fluence of $10 \times 10^{14} \text{ n}_{\text{eq}} \text{ cm}^{-2}$, the sensor requires a bias voltage of 350 V to maintain a gain value same as that of a non-irradiated sensor op-

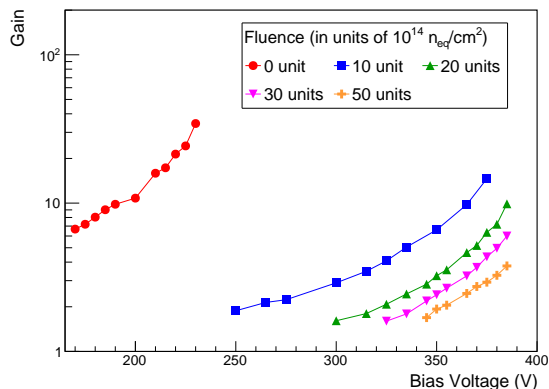


Figure 10: Simulated variation of gain of 20 μm SiC bulk AC-LGAD over a range of operating bias voltage at different fluence levels.

erating at a bias voltage of 150 V. At higher fluence, a comparatively higher V_{bias} is required to compensate for the radiation-induced degradation and maintain the same gain.

It may also be observed that the change in voltage needed to maintain the same gain at high fluence is small in Fig 10. This behavior follows from the exponential acceptor-removal model, described in section 2. At high fluence, further increases in fluence produce smaller changes in doping, so the bias needed to recover the same gain becomes smaller. This explains why the bias curves move closer together at high fluence in Fig 10.

In this study it was also noted that irradiation does not remove the gain layer abruptly. Instead, the peak doping decreases and the multiplication region becomes wider with fluence. For example, at 350 V bias the peak electric field at zero fluence was found to be ≈ 452 kV/cm with a peak acceptor concentration of $\approx 3.7 \times 10^{16}$ cm^{-3} , while at a fluence of 5×10^{15} neq cm^{-2} the peak field decreases to ≈ 201 kV/cm and the peak acceptor concentration to $\approx 2.4 \times 10^{15}$ cm^{-3} . The field remains strong enough for multiplication at high fluence.

4.4.2. Time resolution of irradiated sensors

The timing capability of an irradiated AC-LGAD sensor is studied and compared with that of a non-irradiated one. For this study, again an ultra-thin AC-LGAD with a 20 μm SiC bulk, operated at 243 K is chosen. Figure 11 shows the time resolution against bias voltage for different fluences. The fluence range spans from 10×10^{14} neq cm^{-2} to 50×10^{14} neq cm^{-2} , along with the non-irradiated case.

The red data points in Figure 11, represents the non-

irradiated sensor, which achieves a time resolution below 10 ps. This represents an idealized case, assuming uniform electron-hole pair generation and excluding any random fluctuations in the simulation. The degradation in timing performance is evident when compared to the irradiated sample. Even at relatively low fluence, like 10×10^{14} neq cm^{-2} , there is a noticeable temporal shift, resulting in a clear distinction in timing performance. This degradation is primarily attributed to the acceptor removal mechanism in the gain layer, which reduces internal gain and lowers the signal-to-noise ratio.[20]

For higher fluences, the curves shift towards higher bias voltages in order to achieve improved time resolution. Interestingly, the effect of irradiation appears less pronounced at higher fluences. This can be attributed to the initially higher concentration of boron dopants, which gradually become deactivated as radiation increases, ultimately leaving fewer active atoms susceptible to further effects.

A significant improvement in timing performance is observed as the bias increases from 300 V to 385 V. The most significant changes take place in this range, where the AC-LGAD's ability to resolve time is optimised. At the fluence 20×10^{14} neq cm^{-2} and 50×10^{14} neq cm^{-2} , the time resolution improves by $\sim 77\%$ and $\sim 51\%$ within the voltage difference of $\Delta V = 85$ V and $\Delta V = 40$ V, respectively. The time resolution of less than 20 ps is achieved beyond 375 V for fluence 50×10^{14} neq cm^{-2} . This demonstrates how, and to what extent, the timing performance can be recovered in a moderately doped AC-LGAD after irradiation.

In addition, the study of radiation tolerance is extended for a comparison with Si bulk AC-LGAD for 10×10^{14} neq cm^{-2} and 50×10^{14} neq cm^{-2} . Figure 12 shows, the SiC based AC-LGAD sensors consistently outperform the Si one across the bias range. At a bias voltage of 365 V, for a fluence of 10×10^{14} neq cm^{-2} , SiC bulk achieves a $\sim 40\%$ improvement in time resolution as compared to Si. At higher fluence of 50×10^{14} neq cm^{-2} , improvement remains substantial with a $\sim 37\%$ reduction in time resolution value. This behaviour arises primarily from the higher carrier saturation velocity of silicon carbide compared to silicon, which directly enhances timing performance. In addition, the inherently higher atomic displacement energy of SiC, although not explicitly modelled in the present simulation, provides superior resistance to radiation-induced damage in real materials [13]. The enhanced performance of the SiC bulk is therefore expected to be even more pronounced at high fluences.

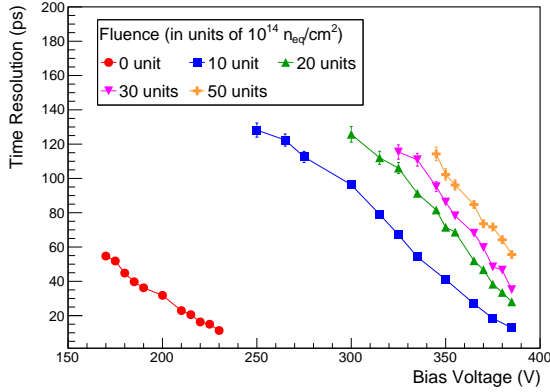


Figure 11: WF2 simulated time resolution of 20 μm SiC bulk AC-LGAD with varying operational bias voltage at different irradianations.

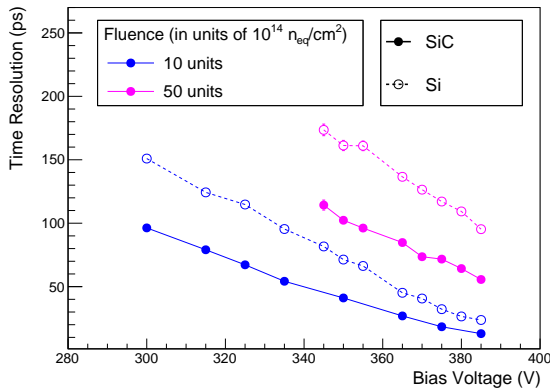


Figure 12: Comparison of WF2 simulated time resolution between a 20 μm SiC and a 20 μm Si bulk AC-LGAD with varying operational bias voltage.

5. Conclusion

This study presents a comprehensive investigation of ultra-thin LGAD sensors using the WeightField2 package. Data from FBK fabricated UFSD devices (silicon (DC) LGAD) are used to compare with WF2 simulation predictions for an identical device and found to be remarkably matching. This validates the effectiveness of WF2 in simulating LGAD devices. In the present study we assumed that the gain layer in 4H-SiC evolves under irradiation in the same way as in silicon. This assumption was necessary due to the lack of available data for irradiated 4H-SiC and in order to compare the two materials within the same simulation framework. We note that this has not yet been verified experimentally and should be considered an open subject for future studies.

It is observed that reducing the sensor thickness from 100 μm to 20 μm , at constant gain values, significantly improves the time resolution by $\sim 60\%$. Furthermore, a simulated SiC sensor achieves around ~ 15 ps better timing performance compared to a silicon device with same gain value ($=10$) and same (very low) thicknesses.

Temperature studies conducted on 20 μm unirradiated SiC sensors show an increase in gain with decreasing temperature, due to increasing ionisation probability at lower temperatures. This increase in gain is further boosted by higher bias voltages, where the time resolution also improves at lower temperatures and higher bias, reaching as low as ~ 13 ps at 360 V. Furthermore, when compared to conventional silicon LGAD sensors, the SiC sensors shows a significant improvement in time resolution of $\sim 40\%$, with decreasing temperature, emphasizing the superior timing response of SiC-based devices.

Radiation tolerance studies confirm significant differences in gain and time resolution between unirradiated sensors and irradiated sensors. The time resolution deteriorates by $\sim 88\%$ for minimum to maximum fluence (irradiated case). The effect is reduced for higher bias voltages, and a time resolution of ~ 55 ps could be achieved for SiC bulk AC-LGAD at highest fluence by optimising operational parameters. Similar comparative study for the minimum and maximum fluence levels for Si bulk LGAD shows a deterioration of $\sim 72\%$ in time resolution in Si bulk at highest fluence when compared to SiC.

This paper has further shown the feasibility of significant enhancements in the gain and the time resolution at optimised sensor thickness and operating temperatures, with robust performance maintained even under a high radiation regime. Having already shown better performance of SiC LGAD device over a conven-

tional Si LGAD device, we conclude that a fabricated ultra-thin SiC UFSD will demonstrate considerable superiority over Si sensors. This study aims to present a benchmark for comparison with future SiC AC-LGAD devices fabricated for 4D tracking applications under extreme conditions.

Acknowledgments

The authors gratefully acknowledge the Weightfield2 simulation package and sincerely thank its developers for making it freely available to the scientific community. P. Palni and J. Kalani would also like to thank the SPS local cluster facility and the IIT Mandi SRIC seed grant support (Ref. No. IITM/SG/PP/128), they acknowledge the National Supercomputing Mission (NSM) for providing computing resources of 'PARAM Himalaya' at IIT Mandi, which is implemented by C-DAC and supported by the Ministry of Electronics and Information Technology (MeitY) and the Department of Science and Technology (DST), Government of India. S. Datta and G. J. Tambave acknowledge the infrastructure support of NISER, which is an OCI under Homi Bhabha National Institute; they acknowledge the funding of the Department of Atomic Energy, Government of India.

Appendix

Table 1: Simulation parameters and their values for the FBK device experimental verification. (Fig 2)

Sr. No.	Parameter	Value
1	Bulk Material	Si
2	Structure	DC-LGAD
3	Number of strips	1
4	Thickness	55 μm
5	Gain Layer Implant (GL)	0.5-1 μm
6	Gain Dopant	B + C
7	Gain Layer Doping	$4.71 \times 10^{16} \text{ cm}^{-3}$
8	Acceptor Removal (Doping Removal)	Kept ON (For irradiated samples)
9	No. of e^-/h^+ Produced	75 / μm (Uniform distribution)
10	Temperature	253 K (For irradiated samples) and 293 K (For unirradiated samples)
11	Fluence	Varied as per reference study

Table 2: Simulation parameters and their values used in the study of choice of bulk material. (Fig 3)

Sr. No.	Parameter	Value
1	Detector Type	AC-LGAD
2	Bulk Material	SiC / Si / Diamond
3	Number of strips	3
4	Detector Thickness	20 μm
5	Gain Layer Implant (GL)	0.5-1 μm
6	Gain Doping	4.3 (for SiC), 4.422 (for Si), 4.43 (for Diamond) (in units of $10^{16} n_{eq} \text{ cm}^{-3}$)
7	Bias Voltage	150 V
8	No. of e^-/h^+ Produced	57 / μm (SiC), 75 / μm (Si), 40 / μm (Diamond) (Uniform ionization)
9	Temperature	243 K
10	Trapping Coefficients	$\beta_e = 4.9 \times 10^{-16} \text{ cm}^2/\text{ns}$, $\beta_h = 6.2 \times 10^{-16} \text{ cm}^2/\text{ns}$

Table 3: Simulation parameters and their values used in the thickness study for SiC AC-LGADs. (Fig 4)

Sr. No.	Parameter	Value
1	Detector Type	AC-LGAD
2	Bulk Material	SiC
3	Number of strips	5
4	Gain Layer Implant (GL)	0.5-1 μm
5	Gain Doping	Varied concentrations of Boron
6	Bias Voltage	300 V
7	No. of e^-/h^+ Produced	57 / μm (SiC, Uniform ionization)
8	Temperature	243 K (Common simulation temperature)

Table 4: Simulation parameters and their settings used in the thickness study for Si and SiC AC-LGADs, gain comparison. (Fig 5,6)

Sr. No.	Parameter	Value
1	Detector Type	AC-LGAD
2	Bulk Material	Si / SiC
3	Number of strips	5
4	Thickness	20-100 μm (Different active layer thicknesses simulated)
5	Gain Layer Implant (GL)	0.5-1 μm
6	Gain Doping	$\sim (2.8-5.0) \times 10^{16} \text{ cm}^{-3}$ Boron atoms
7	Bias Voltage	300 V
8	No. of e^-/h^+ Produced	57 / μm (SiC), 75 / μm (Si) (Uniform ionization)
9	Temperature	243 K (Common simulation temperature)

Table 5: Simulation parameters and their values used in the temperature study for SiC AC-LGAD gain. (Fig 7)

Sr. No.	Parameter	Value
1	Detector Type	AC-LGAD
2	Bulk Material	SiC
3	Number of strips	5
4	Thickness	20 μm (ultra-thin)
5	Gain Layer Implant (GL)	0.5-1 μm
6	Gain Doping	$2.301 \times 10^{16} \text{ cm}^{-3}$ (Boron atoms)
7	No. of e^-/h^+ Produced	57 / μm (SiC, Uniform ionization)

Table 6: Simulation parameters and their values used in the temperature study for Si and SiC AC-LGADs, time resolution comparison. (Fig 8)

Sr. No.	Parameter	Value
1	Detector Type	AC-LGAD
2	Bulk Material	SiC / Si
3	Number of strips	5
4	Thickness	20 μm (ultra-thin)
5	Gain Layer Implant (GL)	0.5-1 μm
6	Gain layer doping	$2.301 \times 10^{16} \text{ cm}^{-3}$ (Boron atoms)
7	No. of e^-/h^+ Produced	57 / μm (SiC), 75 / μm (Si) (Uniform ionization)

Table 7: Simulation parameters and their values used in the thickness-fluence study of SiC AC-LGADs. (Fig 9)

Sr. No.	Parameter	Value
1	Detector Type	AC-LGAD
2	Bulk Material	SiC
3	Number of strips	1
4	Thickness	20-120 μm
5	Gain Layer Implant (GL)	0.5-1 μm
6	Gain layer doping	$4.40 - 4.94 \times 10^{16} \text{ cm}^{-3}$ (Boron atoms)
7	No. of e^-/h^+ Produced	57 / μm uniform ionisation for SiC
8	Temperature	253 K
9	Bias Voltage	115-200 V

Table 8: Simulation parameters and their values used in the radiation hardness study for SiC AC-LGADs and comparison with Si (Fig.10, 11, 12).

Sr. No.	Parameter	Value
1	Detector Type	AC-LGAD
2	Bulk Material	SiC / Si
3	Number of Strips	5
4	Thickness	20 μm (Ultra-thin)
5	Gain Layer Implant (GL)	0.5-1 μm
6	Gain Doping	$3.701 \times 10^{16} \text{ cm}^{-3}$ (Boron doped)
7	Acceptor Removal	Kept ON
8	Trapping Coefficients	$\beta_e = 4.9 \times 10^{-16} \text{ cm}^2/\text{ns}$, $\beta_h = 6.2 \times 10^{-16} \text{ cm}^2/\text{ns}$
9	Temperature	243 K (Common)
10	No. of e^-/h^+ Produced	57 / μm (SiC), 75 / μm (Si) (Uniform ionization)

References

- [1] B. Schmidt *et al.*, The High-Luminosity upgrade of the LHC: Physics and Technology Challenges for the Accelerator and the Experiments, *J. Phys.: Conf. Ser.* 706 (2016) 022002, doi:10.1088/1742-6596/706/2/022002
- [2] A. Abada *et al.* FCC-ee: The Lepton Collider: Future Circular Collider Conceptual Design, *Report Volume 2*. *Eur. Phys. J. ST*, 228(2):261–623, 2019.
- [3] A. Abada *et al.*, FCC-hh: The Hadron Collider: Future Circular Collider Conceptual Design, *Report Volume 3*. *Eur. Phys. J. ST*, 228(4):755–1107, 2019.
- [4] A. Deshpande, The Electron Ion Collider (EIC): Science and Status, *XX-th International Workshop on Hadron Structure and Spectroscopy, Yerevan, 2024*.
- [5] Marco Ferrero, Roberta Arcidiacono, *et al.*, An Introduction to Ultra-Fast Silicon Detectors, *CRC Press*, 2021.
- [6] S. Wada, K. Onaru, *et al.*, Design of a Segmented LGAD Sensor for the Development of a 4-D Tracking Detector, *Proceedings of Science, vol. Vertex2019*, 2020.
- [7] G. D’Amen, W. Chen, G. Giacomini, *et al.*, Measurements of time and spatial resolution of AC-LGADs with different designs, *Journal of Instrumentation, Volume 7, August 2022*
- [8] CMS collaboration. Technical Proposal for a MIP Timing Detector in the CMS Experiment Phase 2 Upgrade, *Technical Report, 2017, CERN Document Server*
- [9] CMS Collaboration, A MIP Timing Detector for the CMS Phase-2 Upgrade, CERN-LHCC-2019-003, CMS-TDR-020 (2019), <https://cds.cern.ch/record/2676871>.
- [10] ATLAS collaboration. Technical Proposal: A High-Granularity Timing Detector for the ATLAS Phase-II Upgrade, *Technical Report, CERN-LHCC-2018-023, LHCC-P-012, CERN Document Server*
- [11] A. Sarkar, P. Palni, S.K. Das, J. Kalani *et al.*, Dynamics of hot QCD matter 2024 - new facilities and instrumentation, *Int. J. Mod. Phys. E* 34 (2025) 2544001.
- [12] N. Cartiglia *et al.*, LGAD designs for future particle trackers, *Nucl. Instrum. Meth. A* 978 (2020), 164383 doi:10.1016/j.nima.2020.164383.
- [13] M. De Napoli, SiC detectors: A review on the use of silicon carbide as radiation detection material, *Front. Phys.* 10 (2022) 898833, doi:10.3389/fphy.2022.898833.
- [14] Y. Satapathy, B.J. Sekely, A. Tishelman-Charny, T. Yang, G. Allion, G. Atar, P. Barletta, C. Haber, S.E. Holland, J.F. Muth, S. Pavlidis and S. Stucci, Impact of Proton Irradiation on 4H-SiC Low Gain Avalanche Detectors (LGADs), *arXiv:2407.02510*.
- [15] Z. He, Review of the Shockley–Ramo theorem and its application in semiconductor gamma-ray detectors, *Nuclear Instruments and Methods in Physics Research A*, vol. 463, pp. 250–267, 2001.
- [16] S. Ramo, Currents induced by electron motion, *Proc. IRE* 27 (1939) 584–585, doi:10.1109/JRPROC.1939.228757.
- [17] H. F.-W. Sadrozinski, A. Seiden, and N. Cartiglia, 4-Dimensional Tracking with Ultra-Fast Silicon Detectors, *Reports on Progress in Physics*, vol. 81, no. 2, p. 026101, 2018.
- [18] N. Cartiglia *et al.*, Design optimization of ultra-fast silicon detectors, *Nuclear Instruments and Methods in Physics Research A*, vol. 796, pp. 141–148, 2015.
- [19] D. J. Massey, J. P. R. David, and G. J. Rees, Temperature Dependence of Impact Ionization in Submicrometer Silicon Devices, *IEEE Transactions on Electron Devices*, vol. 53, no. 9, pp. 2173–2179, September 2006.
- [20] F. Moscatelli *et al.*, TCAD Simulations of Innovative Low-Gain Avalanche Diodes for Particle Detector Design and Optimization, *JPS Conf. Proc.* 42, 011031 (2024), *Proceedings of the 31st International Workshop on Vertex Detectors (VERTEX2022)*
- [21] E. Currás Rivera and M. Moll, Study of Impact Ionization Coefficients in Silicon With Low Gain Avalanche Diodes, *IEEE Transactions on Electron Devices* 70(6), 2919-2926 (2023), *arXiv:2211.16543*

- [22] Carmen Altana *et al.*, Radiation Damage by Heavy Ions in Silicon and Silicon Carbide Detectors, *Sensors*, 2023, 23(14), 6522
- [23] V. V. Emtsev, T. V. Mashovets, V. V. Mikhnovich, N. A. Vitovskii. Frenkel pairs in silicon and germanium, *Radiation Effects and Defects in Solids*, Volume 11-112, 1989
- [24] M. Moll, Acceptor removal – Displacement damage effects involving the shallow acceptor doping of p-type silicon devices, *PoS Vertex2021 (2022)* 017.
- [25] A.A. Lebedev, V.V. Kozlovski *et al.*, Radiation hardness of silicon carbide upon high-temperature electron and proton irradiation, *Materials* 14 (2021) 4976, doi:10.3390/ma14174976.
- [26] F. Hartmann, Evolution of Silicon Sensor Technology in Particle Physics, *Springer Nature, Springer Tracts in Modern Physics*
- [27] N. Cartiglia *et al.*, Performance of ultra-fast silicon detectors, *JINST* 9 (2014) C02001, arXiv:1312.1080.
- [28] F. Cenna *et al.*, Weightfield2: A fast simulator for silicon and diamond solid state detector, *Nuclear Instruments and Methods in Physics Research A*, vol. 796, pp. 149–153, 2015.
- [29] S. Sciortino, S. Lagomarsino, and F. Nava, Silicon Carbide for High Signal to Noise Ratio MIPs Detection From Room Temperature to 80°C, *IEEE Transactions on Nuclear Science*, vol. 56, no. 4, pp. 2538–2542, 2009.
- [30] M. Ferrero *et al.*, Radiation resistant LGAD design, *Nucl. Instrum. Meth. A* 936, 56–67 (2019).
- [31] M. Noy, G. Aglieri Rinella, A. Ceccucci, G. Dellacasa, M. Fiorini *et al.*, The front end electronics of the NA62 gigatracker: Challenges, design and experimental measurements, *Nucl. Phys. B Proc. Suppl.* 215, 198–200 (2011).
- [32] S.M. Mazza *et al.*, Properties of FBK UFSDs after neutron and proton irradiation up to 6×10^{15} neq/cm², *JINST* 15 (2020) T04008
- [33] M. Ferrero, Development of Ultra Fast Silicon Detector for tracking in 4 dimensions, PhD Thesis, University of Torino (2018).
- [34] S. Zhao *et al.*, Charge collection performance of 4H-SiC LGAD, arXiv:2405.18112(2024), doi:10.48550/arXiv.2405.18112.
- [35] J. M. Rafi *et al.*, Electron, neutron, and proton irradiation effects on SiC radiation detectors, *IEEE Trans. Nucl. Sci.* (2020),doi:10.1109/TNS.2020.3029730.
- [36] C. R. Crowell and S. M. Sze, Temperature dependence of avalanche multiplication in semiconductors, *Appl. Phys. Lett.* 9 (1966) 242, doi:10.1063/1.1754704.
- [37] J. Whitmore *et al.*, Radiation validation for the CMS HCAL front-end electronics, *FERMILAB-CONF-10-460-E* (2010).
- [38] N. Boetti, P. Jarron, B. Kisielewski, F. Facio, Radiation performance of the L4913 voltage regulator, *IEEE Trans. Nucl. Sci.* 50 (2003) 2343–2348,doi:10.1109/TNS.2003.820660.
- [39] J. B. Johnson, Thermal agitation of electricity in conductors, *Phys. Rev.* 32 (1928) 97–109,doi:10.1103/PhysRev.32.97.
- [40] V. Raskina *et al.* (ATLAS HGTD Collaboration), Performance studies of the Low Gain Avalanche Detectors for the ATLAS High Granularity Timing Detector in beam tests, *ATL-HGTD-PROC-2022-005*.
- [41] L.A. Beresford *et al.*, Destructive breakdown studies of irradiated LGADs at beam tests for the ATLAS HGTD, *JINST* 18 P07030, doi:10.1088/1748-0221/18/07/P07030.